Deprotonation dynamics of guanine radical cations

Evangelos Balanikas, Akos Banyasz, Gérard Baldacchino, Dimitra Markovitsi

▶ **To cite this version:**

Evangelos Balanikas, Akos Banyasz, Gérard Baldacchino, Dimitra Markovitsi. Deprotonation dynamics of guanine radical cations. Photochemistry and Photobiology, 2022, 98, pp.523-531. 10.1111/php.13540 . cea-03383354

HAL Id: cea-03383354

https://cea.hal.science/cea-03383354

Submitted on 18 Oct 2021

HAL is a multi-disciplinary open access archive for the deposit and dissemination of scientific research documents, whether they are published or not. The documents may come from teaching and research institutions in France or abroad, or from public or private research centers.

L'archive ouverte pluridisciplinaire **HAL**, est destinée au dépôt et à la diffusion de documents scientifiques de niveau recherche, publiés ou non, émanant des établissements d'enseignement et de recherche français ou étrangers, des laboratoires publics ou privés.

Copyright

Deprotonation dynamics of guanine radical cations

Evangelos Balanikas[1], Akos Banyasz[1,2], Gérard Baldacchino[1] and Dimitra Markovitsi*[1],

[1]. Université Paris-Saclay, CEA, CNRS, LIDYL, F-91191 Gif-sur-Yvette, France,

[2]. Univ Lyon, ENS de Lyon, CNRS UMR 5182, Université Claude Bernard Lyon 1, Laboratoire de Chimie, F-69342 Lyon, France

*Corresponding author e-mail: dimitra.markovitsi@cea.fr (Dimitra Markovitsi)

ABSTRACT

This review is dedicated to guanine radical cations $(G^{+})^{\bullet}$ that are precursors to oxidatively generated damage to DNA. $(G^{+})^{\bullet}$ are unstable in neutral aqueous solution and tend to lose a proton. The deprotonation process has been studied by time-resolved absorption experiments in which $(G^{+})^{\bullet}$ radicals are produced either by an electron abstraction reaction, using an external oxidant, or by low-energy/low-intensity photoionization of DNA. Both the position of the released proton and the dynamics of the process depend on the secondary DNA structure. While deprotonation in duplex DNA leads to $(G\text{-}H1)^{\bullet}$ radicals, in guanine quadruplexes the $(G\text{-}H2)^{\bullet}$ analogues are observed. Deprotonation in monomeric guanosine proceeds with a time constant of ~60 ns, in genomic DNA is completed within 2 μs and spans from at least 30 ns to over 50 μs in guanine quadruplexes. Such a deprotonation dynamics in four-stranded structures, extended over more than three decades of times, is correlated with the anisotropic structure of DNA and the mobility of its hydration shell. In this case, commonly used second order reaction models are inappropriate for its description.

INTRODUCTION

Guanine radical cations $(G^{+})^{\bullet}$ are precursors to DNA damage under oxidative stress (1). These species are unstable in neutral aqueous solutions and tend to lose a proton, giving rise to deprotonated guanine radicals $(G\text{-}H)^{\bullet}$ (2). Alternatively, $(G^{+})^{\bullet}$ may follow other reaction path; for example, undergo hydration, which subsequently leads to the well-known oxidation marker 8-oxo-7,8-dihydro-2'-deoxyguanosine (8-oxodG) (1). The relative yields of the final lesions resulting from various reactions in competition depend, among others, on the dynamics of the associated reactions. In other terms, the faster the reaction rate, the higher the probability to observe lesions resulting from this reaction (3).

Information about the deprotonation dynamics of $(G^{+})^{\bullet}$ in room temperature solutions has been obtained by time-resolved techniques, pulsed radiolysis (4, 5) and flash photolysis (6-13), probing the absorption of guanine radicals on the UV-visible spectral domain. Depending on the way in which the $(G^{+})^{\bullet}$ are generated, we can distinguish two main experimental approaches. On the one hand, $(G^{+})^{\bullet}$ may be produced by electron abstraction from DNA through a reaction with an external oxidant; this approach is named hereafter "indirect". On the other, $(G^{+})^{\bullet}$ may result from photoionization of DNA, without mediation of other molecules, which we coin "direct" approach.

In 1992, Candeias and Steenken observed that radicals of monomeric guanosine derivatives generated by photoionization in neutral aqueous solutions are already deprotonated in 200 ns (14). The first determination of $(G^{+})^{\bullet}$ deprotonation dynamics was achieved a decade later by Kobayashi and Tagawa (4). This study, as well as subsequent ones performed for different

types of DNA multimers, revealed that the $(G^+)^\bullet$ deprotonation rate strongly depends on the secondary structure (4, 6-9, 11-13). Despite the qualitative agreement of the findings published by various groups, important discrepancies regarding the reported rate or time constants appeared, mostly in the case of guanine quadruplexes (G-Quadruplexes). These four-stranded DNA structures are formed by folding and/or association of guanine rich DNA/RNA strands in the presence of metal cations (Figure 1); the latter affect both the folding geometry and the stability of the resulting scaffold (15). G-Quadruplexes are extensively studied because of their important role in numerous biological functions (16, 17) and their potential applications in biosensors (18-20).

>Figure 1<

The objective of the present review is to (i) highlight the major outcomes on the dynamics of $(G^+)^\bullet$ deprotonation in neutral aqueous solutions reported from different groups, (ii) compare the conclusions reached following different experimental methodologies and (iii) discuss the origins for the observed inconsistencies. As experiments providing information on reaction dynamics require the knowledge of the absorption spectra of the radicals, we start our review by presenting their features. In a next step, the basic principles underlying direct and indirect $(G^+)^\bullet$ generation are outlined. Then, we present the main results acquired by both indirect and direct approaches. The latter were obtained in our group exploiting a recently discovered unexpected phenomenon: absorption directly by DNA of single photons with energies significantly lower compared to the vertical ionization potential of nucleobases (21) may provoke electron ejection (22-24, 13, 25). The photoionization process as well as the general methodology adopted for the quantification of the ejected electrons and guanine radicals have

been recently highlighted (13). Here, we insist on quantitative aspects related to the deprotonation dynamics, enriching the existing picture with a novel methodology for the determination of the $(G^{+})^{\bullet}$ survival probability in G-Quadruplexes. Finally, after comparing the various findings, we discuss the occurrence of non-constant reaction rates involving DNA.

ABSORPTION SPECTRA: A PREREQUISITE FOR DYNAMICAL STUDIES

The absorption spectra of both $(G^{+})^{\bullet}$ and the resulting deprotonated radicals were first determined by Candeias and Steenken (26). In the case of the nucleoside (dG) and nucleotide (dGMP), they found that the proton in position 1 of the guanine is lost upon deprotonation; but if the release of this proton is not possible, as happens in the case of 1-methyl guanine, the proton in position 2 of the amino group takes over (Figure 2, insets). The ensued deprotonated radicals, noted $(G\text{-}H1)^{\bullet}$ and $(G\text{-}H2)^{\bullet}$, respectively, exhibit quite different absorption spectra. As the relevant feature for the determination of the deprotonation dynamics is the spectral change occurring during this process, we present in Figure 2 the differential spectra corresponding to $(G^{+})^{\bullet} \rightarrow (G\text{-}H1)^{\bullet}$ and $(G^{+})^{\bullet} \rightarrow (G\text{-}H2)^{\bullet}$ deprotonations.

>Figure 2<

The spectral features of the various guanine radicals were recently rationalized by quantum chemistry calculations (27, 28). In addition, these studies showed, that their main characteristics in the visible spectral domain are maintained upon hydrogen-bonding and base-stacking. Computations also indicated subtle differences in duplex spectra depending on

whether the H1 proton is transferred either to the bulk water or to the cytosine (Figure 3a). However, the sensitivity of time-resolved measurements does not allow a clear distinction between these two transfers.

Globally, the spectra of deprotonated radicals in DNA multimers match quite well those of monomeric guanosine in the visible spectral domain (9, 13). But moving towards the UV, the agreement may be less good, because of the contribution of the "initial" multimer absorption (see Figure 9 in reference (7)). As a matter of fact, due to the electronic coupling among nucleobases, the Franck-Condon excited states of DNA multimers differ from those of non-interacting monomers (29, 30, 28, 31) and this is reflected in their time-resolved absorption spectra.

>Figure 3<

The absorption spectra of $(G^{+})^{\bullet}$ in certain G-Quadruplexes were determined experimentally for solutions with pH 3, where deprotonation is known to be hindered for monomeric guanosine derivatives (26). It was observed that the spectral intensity below 450 nm is significantly lower than that of the monomeric analogue (7, 9). This finding is supported by quantum chemistry computations (7, 28), which also showed that the electron hole may be delocalized over parallel stacked guanines (32-36, 28). Such a delocalization could influence the deprotonation rate. However, its occurrence has not been clearly established on the time-scales and temperatures discussed here.

GENERATION OF RADICAL CATIONS

All the studies that reported deprotonation dynamics following the indirect approach, used $(SO_4^{-})^{\bullet}$ as external oxidant to produce $(G^{\bullet})^{+}$ radicals.

$$(SO_4^{-})^{\bullet} + G \rightarrow SO_4^{2-} + (G^{\bullet})^{+} \quad \text{(reaction I).}$$

The oxidant itself is formed from a peroxodisulfate salt via a two-step or one-step process. In pulsed radiolysis (4, 5), first, the interaction of an electron beam with water gives rise to hydrated electrons e_{hyd}^{-} and $HO^{\bullet}$ radicals. The latter are scavenged by tert-butyl alcohol, which is also added in the solution so that to avoid their reaction with DNA. Then, hydrated electrons react with peroxodisulfate anions:

$$e_{hyd}^{-} + S_2O_8^{2-} \rightarrow SO_4^{2-} + (SO_4^{-})^{\bullet} \quad \text{(reaction II).}$$

If laser irradiation is used instead of an electron beam, the oxidant is generated by a single photochemical reaction (6, 10):

$$h\nu + S_2O_8^{2-} \rightarrow 2(SO_4^{-})^{\bullet} \quad \text{(reaction III).}$$

In the low-energy photoionization studies, $(G^{\bullet})^{+}$ generation takes place at 266 nm (13). The key point of this approach is the use of laser intensities ($\leq 2\times10^{6}$ Wcm^{-2}) significantly lower compared to those used to study final lesions (37). Under these conditions, the e_{hyd}^{-} originate only from DNA, without interference from solvent ionization. Consequently, they can be quantified and compared with the radical concentration through the corresponding molar absorption coefficients (ε) as explained in reference (13). For the experiments reported here, DNA was dissolved in the phosphate buffer, composed of an equimolar mixture of NaH_2PO_4/Na_2HPO_4 or KH_2PO_4/K_2HPO_4 in concentrations of 0.015 - 0.15 $mol\cdot L^{-1}$ each. Under these conditions, e_{hyd}^{-} decay in less than 2 μs, reacting with $H_2PO_4^{-2}$ (13).

We remark that, going from pulse radiolysis to photosensitized electron abstraction and further to photoionization, both the number of reaction steps necessary to generate $(G^{\bullet})^{+}$ and the number of chemicals present in the solution, decrease. The counterpart is that, in parallel, the

intensity of the transient absorption signals decreases, typically by two orders of magnitude (compare, for example, Figure 5 in reference (4) and Figure 4 in this manuscript). Therefore, low-energy photoionization studies require long measurement times. In addition, both DNA and the buffer ingredients need to be purified so that to avoid spurious signals from impurities and/or their interaction with radicals.

We stress that the initial electron holes generated by either the indirect or the direct method are not necessarily located on guanine sites. On the one hand, $(SO_4^-)^\bullet$ may oxidize other nucleobases (38, 39), and, on the other, low-energy photoionization takes place also in DNA multimers devoid of guanines (23, 24). But, as guanine has the lowest oxidation potential among nucleobases (40), the electron hole is rapidly trapped by guanines following a charge transport process (41-47) and only guanine radicals are observed in the experiments described here.

MAIN FINDINGS: INDIRECT APPROACH

In their seminal work, Kobayashi and Tagawa (4) performed pulse radiolysis and probed the transient absorption at 625 nm (see Figure 2a). They found that $(G^+)^\bullet \rightarrow (G\text{-}H1)^\bullet$ deprotonation in dG proceeds with a rate constant of 1.8×10^7 s^{-1} (56 ns). Recent flash photolysis measurements yielded a similar rate constant (1.5×10^7 s^{-1} / 67 ns) (10).

Kobayashi and Tagawa also studied the deprotonation dynamics of $(G^+)^\bullet$ in a series of model duplexes with 12-13 base-pairs containing G, GG and GGG steps at different positions (4). In this case, the fit of the transient signals required two-exponential functions, provided rate constants of 1.3×10^7 s^{-1} (78 ns) and 3×10^6 s^{-1} (330 ns). The fastest one was attributed to

guanines located close to the ends of the duplex, while the slowest was assigned to internal guanine sites.

The first study on G-Quadruplexes was performed by Su and co-workers, using photosensitized electron abstraction (6). They examined four different sequences forming monomolecular, bimolecular and tetramolecular structures (Figure 1). They came to two important conclusions. First, they showed that, in contrast to what was observed for duplexes, $(G^{+})^{\bullet}$ deprotonation in these systems does not involve release of the H1 proton but of the H2 proton (Figure 1b). This conclusion was attested by the appearance in the transient absorption spectra of a band peaking in the red, which is typical of the $(G\text{-}H2)^{\bullet}$ radicals (26, 48). It was explained by the fact that H1 protons are engaged in the Hoogsteen hydrogen bonds connecting the guanines within the guanine tetrads (Figure 3b). Later, quantum chemistry calculations found that, indeed, $(G\text{-}H2)^{\bullet}$ radicals in G-quadruplexes are more stable than the $(G\text{-}H1)^{\bullet}$ analogues (9). The second conclusion was that $(G^{+})^{\bullet} \rightarrow (G\text{-}H2)^{\bullet}$ deprotonation in G-Quadruplexes is slower compared to $(G^{+})^{\bullet} \rightarrow (G\text{-}H1)^{\bullet}$ in duplexes. Rate constants ranging from $1.4\times10^{6}\ s^{-1}$ (0.7 μs) and $2\times10^{5}\ s^{-1}$ (5 μs) were reported.

A subsequent study on two G-quadruplexes, also performed by photosensitized electron abstraction reached a different conclusion (49). The transient absorption spectra recorded at 50 μs were attributed to $(G\text{-}H1)^{\bullet}$ deprotonated radicals but the discrepancy with previously reported studies (6, 7) was not discussed.

MAIN FINDINGS: DIRECT APPROACH

In photoionization studies, a full spectral characterization of the radicals is possible only after 2-3 μs. This is due, on the one hand, to the low intensity of the transient absorption signals, which are noisier on shorter times, and, on the other, to the presence of hydrated ejected electrons, whose broad and intense absorption is extended over the whole visible domain (13). Yet, some delicate measurements were performed on the sub-microsecond time-scale by adding in the solution efficient electron scavengers, N_2O or NO_3^- (50).

For all the DNA systems studied by this method, the guanine radical concentration at 2-3 μs was found to be equal to that of the hydrated ejected electrons $[e_{hyd}^-]_0$, determined by independent experiments on the sub-microsecond time-scale (13). Thus, it was possible to quantitatively follow the entire radical population during the time. We note that these "initial" concentrations correspond to electron and holes that escaped recombination (51) and may provoke DNA damage.

The differential absorption spectra recorded on the microsecond time-scale for model duplexes and purified calf thymus DNA (CT-DNA) (52, 8, 13) correspond to that of $(G\text{-}H1)^\bullet$ radicals, showing that $(G^+)^\bullet \rightarrow (G\text{-}H1)^\bullet$ deprotonation takes place earlier. The deprotonation dynamics was determined in the case of CT-DNA by recording transient absorption signals at 700 nm. The latter exhibit a rise, which can be described by a mono-exponential function with a time constant of 320 ± 30 ns ns; after 2μs, the signal starts decreasing slowly (Figure 4) and subsequently it decays on the millisecond time-scale (13).

>Figure 4<

192 A more complex picture was found in the case of G-Quadruplexes. The study of 7 different
193 systems showed that a significant population of the initially generated $(G^{+})^{\bullet}$ is still present at 3
194 μs (Table 1). Depending on the G-quadruplex type, the concentration of this "long-lived" $(G^{+})^{\bullet}$
195 population varies from 25% to 60% of $[e_{hyd}^{-}]_0$ while the remaining part corresponds to $(G\text{-}H2)^{\bullet}$
196 radicals.

197 >Table 1<

198 The percentages presented in Table 1 were determined by reconstructing the transient
199 absorption spectra obtained for the studied G-Quadruplexes by linear combinations of the
200 spectra reported for monomeric guanosine radicals the $(G^{+})^{\bullet}$ and $(G\text{-}H2)^{\bullet}$. This reconstruction
201 takes into account not only the spectral shape but also the spectral intensities. To this end, the
202 differential absorption ΔA, observed over an optical path-length of 1 cm, was divided by the
203 concentration of hydrated ejected electrons, while the monomer spectra were considered with
204 their ε (26). An example is given in Figure 5a where the transient absorption spectrum of
205 OXY/Na^{+} at 3 μs is presented together with that corresponding of a linear combination of $(G^{+})^{\bullet}$
206 and $(G\text{-}H2)^{\bullet}$ radicals at a ratio of 45/55 while the sum of their concentrations is equal to the
207 detected $[e_{hyd}^{-}]_0$.

208 >Figure 5<

209 For some G-Quadruplexes, deprotonation toward $(G\text{-}H2)^{\bullet}$ becomes much more obvious on
210 later times. For example, the spectrum of $(TG_4T)_4/Na^{+}$ at 50 μs (Figure 5 in reference (9))
211 strongly resembles that of monomeric $(G\text{-}H2)^{\bullet}$. At even longer times, $(G\text{-}H2)^{\bullet} \rightarrow (G\text{-}H1)^{\bullet}$

tautomerization, which is in competition with other reaction paths, may be observed (13). But this aspect is out of the scope of the present review.

>Figure 6<

For a few cases, the early deprotonation dynamics could be resolved. This is presented in Figure 6 for TEL21/K^+, OXY/Na^+ and OXY/K^+: the transient signals recorded at 620 nm exhibit a rise, corresponding to the appearance of $(G\text{-}H2)^\bullet$ radicals (see Figure 2b). Although these signals are very noisy, it is clear that a fast deprotonation process takes place in less than 1 μs; the time constants, derived from fits with mono-exponential functions (150 ± 15 ns in Figure 6a and 200 ± 30 ns in Figure 6b), are smaller than that found for CT-DNA (320 ± 30 ns, Figure 4).

Coming to the slow deprotonation process, it could be visualized directly by transient absorption signals only in the case of tetramolecular G-quadruplexes (9, 11). For these systems, the $(G\text{-}H2)^\bullet$ population at 50 μs is still equal to that of the total radical population at 3 μs. Thus, the decay of the differential absorbance at 500 nm and the rise at 600 nm reflect directly the deprotonation dynamics. This is shown in Figure 7a for $(TG_4T)_4/Na^+$, where both the decay and the rise are approximated by single exponential functions, with the same time constant of 6 ± 1 μs (9). The deprotonation is practically completed at 20 μs. For other systems, the total radical population, determined by the transient absorption decays at 510-515 nm as explained in reference (13), starts decreasing before completion of the deprotonation processes. For this reason, a different method was adopted in order to determine the reaction dynamics of $(G^+)^\bullet$. Several time-resolved spectra were recorded on the microsecond time-scale and, subsequently, reconstructed in the same way as that followed for the 3 μs spectra. As

example is presented in Figure 5b the reconstruction of the spectra recorded for TEL21/Na^+ at 25 μs. At this time, the total radical concentration corresponds to 85% of the hydrated ejected electrons; the missing part was associated with formation of 8-oxodG which was detected by analytical methods (7). Finally, the $(G^+)^\bullet$ survival probability, determined as a percentage of the initially generated electron holes that have escaped recombination, equal to $[e_{hyd}^-]_0$, was plotted. Figures 7b and 7c show the results derived from such an analysis performed for the OXY/Na^+ and TEL21/Na^+. At times longer than 50 μs for the former system and 40 μs for the latter, the errors related with the spectral analysis increase to provide reliable data. At those times, about ~10% of the initial population is still present in the G-Quadruplex.

>Figure 7<

COMMON CONCLUSIONS AND DISCREPANCIES

The above described studies carried out by different groups using different approaches lead to some common conclusions regarding the $(G^+)^\bullet$ deprotonation dynamics.

First, similar rate constants were found for deprotonation in dG via the indirect method using either pulse radiolysis (4) and flash photolysis (6). Second, the characteristic time determined by photoionization of CT-DNA (320 ± 30 ns; Figure 4) (13) matches well the longest time constants (330 ns) derived from the study of model duplexes by pulsed radiolysis (4). The shortest time constants reported in the latter study had been correlated with guanines located close to the ends of the duplexes and it is normal that they are not detected for genomic DNA which is very long macromolecule.

Third, the specificity of $(G^{+})^{\bullet}$ deprotonation towards $(G\text{-}H2)^{\bullet}$ in G-Quadruplexes, initially deduced from photosensitized electron abstraction studies, carried out by Su and co-workers (6), was largely confirmed by our photoionization studies (11, 13, 12, 9, 8, 7). And it is important to note that oxidatively generated lesions to DNA resulting from $(G\text{-}H2)^{\bullet}$ radicals have not been documented so far. Yet, a study Merta et al. using, as the Su group, photosensitized electron abstraction (reaction I), failed to detect the presence of $(G\text{-}H2)^{\bullet}$ in telomeric G-Quadruplexes (49).

Another common conclusion drawn by the Su group and our work is that $(G^{+})^{\bullet}$ radicals in G-Quadruplexes are still observed on the microsecond time-scale. But quantification of $(G^{+})^{\bullet}$ population, possible only through photoionization studies, revealed that these "long-lived" species, whose decays were characterized in the 3 - 50 μs interval (Figure 7), represent only part of the initially generated electron holes (see Table 1). As shown in Figures 6a and 6b, an important part of $(G^{+})^{\bullet}$ deprotonates on much shorter times, even faster compared to CT-DNA (Figure 4).

REACTION RATES IN ANISOTROPIC STRUCTURES

In order to understand the discrepancies regarding the rate constants determined for $(G^{+})^{\bullet}$ deprotonation in G-Quadruplexes, a closer look at the reaction mechanism underlying their determination may be informative. Proton transfer from $(G^{+})^{\bullet}$ to water is considered to be a second order reaction. Given that the bulk concentration of water molecules is much higher than that of $(G^{+})^{\bullet}$, this second order reaction is approximated by a pseudo-first order one, as indicated by the fact that the rate constants are expressed in s^{-1} (4, 6, 10). However, the validity of such an approximation requires certain conditions to be fulfilled. The reaction rate needs to

276 be controlled by diffusion of the reactants and the probability of their encounter should be
277 uniform over the three-dimensional space over the time-window of the experimental
278 measurements (53). This is the model of a well-stirred reactor.
279 The conditions corresponding to the simplified pseudo-first order reaction kinetics are far from
280 valid in G-Quadruplexes. As a matter of fact, analysis of several crystal structures revealed the
281 existence of well-defined water networks, whose properties depend on the topology of G-
282 Quadruplex; the primary water molecules may be hydrogen bonded to phosphate and/or sugar
283 groups and even to guanines at the edges of the G-quadruplexes (54).
284 Heterogeneities are encountered not only in the static arrangement of the DNA hydration shell
285 but also on the lability of its water molecules which may be modulated by slow conformational
286 motions of the nucleic acids (55). Interestingly, the hydration cell has been found to be thicker
287 around G-quadruplexes than duplexes and more difficult to be disrupted by solute molecules
288 (56). According to two-dimensional NMR experiments, the residence times of the water
289 molecules belonging to the hydration shell of model duplexes do not exceed 1 ns at room
290 temperature (57, 58). Consequently, these effects should be averaged on the time-scale on
291 which $(G^{+})^{\bullet}$ deprotonation dynamics is detected for CT-DNA by transient absorption (Figure
292 4). In contrast, longer water rotation and residence times, extended on the microsecond time-
293 scale, have been reported for OXY/Na^{+} G-Quadruplexes (59), explaining, at least partly, the
294 observed slower $(G^{+})^{\bullet}$ deprotonation.
295 Second order kinetics in systems with spatial and dynamical heterogeneity may give rise to
296 multiscale survival probabilities of the reactants (60). Such reaction patterns artificially appear
297 to be mono-exponential if the observation and/or analysis of the time-resolved signals is
298 restricted over a small time-window. In addition, different time-windows result to different

299 time constants. It is worth-noticing that multiscale dynamics characterizes also the excited state
300 relaxation in DNA, where electronic coupling, affected by conformational motions among
301 nucleobases (61), is operative (62).

302 Multiscale reaction rates may also concern $(G^{+})^{\bullet}$ generation in DNA multimers using $(SO_4^{-})^{\bullet}$.
303 Reaction I takes place between negatively charged electron acceptors and spatially correlated
304 electron donors located on a polyelectrolyte. It is possible that the rate constants determined for
305 the oxidation process reflect only part of the reaction. In this case, a simple change in the
306 concentration ratios between DNA and the oxidant or the duration of the laser pulse may
307 modify the oxidation rates and, hence, those of deprotonation. This could provide an
308 explanation why $(G\text{-}H2)^{\bullet}$ radicals have gone undetected in one study (49) while they were
309 readily detected in another (6).

310 Focusing on the deprotonation process determined by the photoionization method, the time
311 constants derived from the fits with exponential functions (Figures 4, 6 and 7) do not
312 necessarily correspond to reaction rate constants; they are simply useful for a
313 phenomenological comparison of the transient absorption traces on a given time-window. In
314 this respect, the first photoionization study of G-Quadruplexes reported that $(G^{+})^{\bullet}$ survive in
315 TEL21/Na^{+} on the millisecond time-scale signals (7). This conclusion was based on time
316 constants derived from exponential fits of the transient absorption signals which, following the
317 above reasoning, may lead to erroneous results. The methodology presented here for the
318 determination of the $(G^{+})^{\bullet}$ survival probability (Figure 5b), based on the transient absorption
319 spectra, provided shorter lifetimes. Therefore, we conclude that deprotonation in G-
320 Quadruplexes spans over three orders of magnitude of time, from at least 30 ns to over 50 μs,
321 the limits being determined by the time resolution and the sensitivity of the experimental set-

up. This anisotropic deprotonation dynamics can be also viewed as the occurrence of dynamically anisotropic pKa values.

As analytical formulas derived from simple reaction patterns cannot describe correctly the $(G^{+})^{\bullet}$ deprotonation dynamics, specific theoretical developments are needed blatantly. A first step toward this direction was made in a recent quantum chemical study: it was shown that a cluster of four water molecules must be taken into account to correctly reproduce the temperature dependence of the reaction rates $(G^{+})^{\bullet} \rightarrow (G\text{-}H1)^{\bullet}$ in dG determined experimentally as a function of temperature (10). Regarding DNA multimers, theoretical studies should encompass, in addition, molecular dynamics simulations on tens of microseconds, already used to describe interaction of DNA with biomolecules (63, 64). In this way, it should be possible to establish a correlation between DNA topology and $(G^{+})^{\bullet}$ dynamics.

ACKNOWLEDGMENTS: This work has received funding from the European Union's Horizon 2020 research and innovation programme under the Marie Sklodowska-Curie grant agreement No. 765266 (LightDyNAmics).

REFERENCES

1. Cadet, J., T. Douki and J.-L. Ravanat (2015) Oxidatively Generated Damage to Cellular DNA by UVB and UVA Radiation. *Photochem. Photobiol.* **91,** 140-155.

2. Steenken, S. (1989) Purine-Bases, Nucleosides and Nucleotides - Aqueous-Solution Redox Chemistry and transformation Reactions of their Radical Cations and e- and OH Adducts. *Chem. Rev.* **89,** 503-520.

3. Balanikas, E. and D. Markovitsi (2021) DNA photoionization: from high to low energies. In *DNA Photodamage*. (Edited by R. Improta and T. Douki), pp. 37-54. RSC, Cambridge.

4. Kobayashi, K. and S. Tagawa (2003) Direct observation of guanine radical cation deprotonation in duplex DNA using pulse radiolysis. *J. Am. Chem. Soc.* **125,** 10213-10218.

5. Choi, J., C. Yang, M. Fujitsuka, S. Tojo, H. Ihee and T. Majima (2015) Proton Transfer of Guanine Radical Cations Studied by Time-Resolved Resonance Raman Spectroscopy Combined with Pulse Radiolysis. *J. Phys. Chem. Lett.* **6,** 5045-5050.

6. Wu, L. D., K. H. Liu, J. L. Jie, D. Song and H. M. Su (2015) Direct Observation of Guanine Radical Cation Deprotonation in G-Quadruplex DNA. *J. Am. Chem. Soc.* **137,** 259-266.

7. Banyasz, A., L. Martinez-Fernandez, C. Balty, M. Perron, T. Douki, R. Improta and D. Markovitsi (2017) Absorption of Low-Energy UV Radiation by Human Telomere G-Quadruplexes Generates Long-Lived Guanine Radical Cations. *J. Am. Chem. Soc.* **139,** 10561-10568.

8. Balanikas, E., A. Banyasz, G. Baldacchino and D. Markovitsi (2019) Populations and Dynamics of Guanine Radicals in DNA strands: Direct versus Indirect Generation. *Molecules* **24,** 2347.

9. Banyasz, A., E. Balanikas, L. Martinez-Fernandez, G. Baldacchino, T. Douki, R. Improta and D. Markovitsi (2019) Radicals generated in tetramolecular guanine quadruplexes by photo-ionization: spectral and dynamical features. *J. Phys. Chem. B* **123,** 4950-4957.

10. Zhang, X., J. Jie, D. Song and H. Su (2020) Deprotonation of Guanine Radical Cation G(center dot+) Mediated by the Protonated Water Cluster. *J. Phys. Chem. A* **124,** 6076-6083.

11. Behmand, B., E. Balanikas, L. Martinez-Fernandez, R. Improta, A. Banyasz, G. Baldacchino and D. Markovitsi (2020) Potassium Ions Enhance Guanine Radical Generation upon Absorption of Low-Energy Photons by G-quadruplexes and Modify Their Reactivity. *J. Phys. Chem. Lett.* **11,** 1305−1309.

12. Balanikas, E., A. Banyasz, G. Baldacchino and D. Markovitsi (2020) Guanine Radicals Generated in Telomeric G-quadruplexes by Direct Absorption of Low-Energy UV Photons: Effect of Potassium Ions. *Molecules* **25,** 2094.

13. Balanikas, E., A. Banyasz, T. Douki, G. Baldacchino and D. Markovitsi (2020) Guanine Radicals Induced in DNA by Low-Energy Photoionization. *Acc. Chem. Res.* **53,** 1511-1519.

14. Candeias, L. P. and S. Steenken (1992) Ionization of purine nucleosides and nucleotides and their components by 193-nm laser photolysis in aqueous solution: model studies for oxidative damage of DNA. *J. Am. Chem. Soc.* **114,** 699-704.

15. Hud, V. and J. Plavec (2006) The role of cations in determining quadruplex structure and stability. In *Quadruplex nucleic acids*. (Edited by S. Balasubramanian and S. Neidle), pp. 100-130. RSC Publishing, Cambridge.

16. Rhodes, D. and H. J. Lipps (2015) G-quadruplexes and their regulatory roles in biology. *Nucleic Acids Res.* **43,** 8627-8637.

17. Kharel, P., G. Becker, V. Tsvetkov and P. Ivanov (2020) Properties and biological impact of RNA G-quadruplexes: from order to turmoil and back. *Nucleic Acids Res.* **48,** 12534-12555.

18. Xiang, X., Y. Li, L. Ling, Y. Bao, Y. Su and X. Guo (2019) Label-free and dye-free detection of target DNA based on intrinsic fluorescence of the (3+1) interlocked bimolecular G-quadruplexes. *Sens. Actuators B Chem.* **290,** 68-72.

19. Liu, T. L., D. X. Sun, M. M. Gu, X. M. Wu and G. L. Wang (2020) Intercalative methylene blue as an efficient signal molecule of tremella-like Bi 2 WO 6: Toward high performance photoelectrochemical biosensing. *Sens. Actuators B Chem.* **317**.

20. Gu, M., D. Sun, T. Liu, X. Wu and G.-L. Wang (2020) Homogenous cathodic photoelectrochemistry for DNA binding protein analysis. *Sens. Actuators B Chem.* **324**.

21. Pluharova, E., P. Slavicek and P. Jungwirth (2015) Modeling Photoionization of Aqueous DNA and Its Components. *Acc. Chem. Res.* **48,** 1209-1217.

22. Marguet, S., D. Markovitsi and F. Talbot (2006) One and two photon ionization of DNA single and double helices studied by laser flash photolysis at 266 nm. *J. Phys. Chem. B* **110,** 11037-11039.

23. Banyasz, A., T. Ketola, A. Muñoz-Losa, S. Rishi, A. Adhikary, M. D. Sevilla, L. Martinez-Fernandez, R. Improrta and D. Markovitsi (2016) UV-induced Adenine Radicals Induced in DNA A-tracts: Spectral and Dynamical Characterization *J. Phys. Chem. Lett.* **7,** 3949-3953.

24. Banyasz, A., T. Ketola, L. Martinez-Fernandez, R. Improta and D. Markovitsi (2018) Adenine radicals generated in alternating AT duplexes by direct absorption of low-energy UV radiation. *Faraday Disc.* **207,** 181-197.

25. Balanikas, E., L. Martinez-Fernadez, R. Improta, P. Podbevsek, G. Baldacchino and D. Markovitsi (2021) The Structural Duality of Nucleobases in Guanine Quadruplexes Controls Their Low-Energy Photoionization. *J. Phys. Chem. Lett.* **12,** 8309−8313.

26. Candeias, L. P. and S. Steenken (1989) Stucture and acid-base properties of one-electron-oxidized deoxyguanosine, guanosine, and 1-methylguanosine. *J. Am. Chem. Soc.* **111,** 1094-1099.

27. Kumar, A. and M. D. Sevilla (2019) Excited States of One-Electron Oxidized Guanine-Cytosine Base Pair Radicals: A Time Dependent Density Functional Theory Study. *J. Phys. Chem. A* **123,** 3098-3108.

28. Martinez-Fernandez, L., L. Esposito and R. Improta (2020) Studying the excited electronic states of guanine rich DNA quadruplexes by quantum mechanical methods: main achievements and perspectives. *Photochem. Photobiol. Sci.* **19,** 436-444.

29. Emanuele, E., K. Zakrzewska, D. Markovitsi, R. Lavery and P. Millie (2005) Exciton states of dynamic DNA double helices: alternating dCdG sequences. *J. Phys. Chem. B* **109,** 16109-16118.

30. Nogueira, J. J., F. Plasser and L. Gonzalez (2017) Electronic delocalization, charge transfer and hypochromism in the UV absorption spectrum of polyadenine unravelled by multiscale computations and quantitative wavefunction analysis. *Chem. Sci.* **8,** 5682-5691.

31. Ibele, L., P. Sánchez-Murcia, S. Mai, J. Nogueira and L. González (2020) Excimer Intermediates en Route to Long-Lived Charge-Transfer States in Single-Stranded Adenine DNA as Revealed by Nonadiabatic Dynamics. *J. Phys. Chem. Lett.* **11,** 7483−7488.

425 32. Adhikary, A., D. Khanduri and M. D. Sevilla (2009) Direct Observation of the Hole
426 Protonation State and Hole Localization Site in DNA-Oligomers. *J. Am. Chem. Soc.* **131,**
427 8614-8619.
428 33. Adhikary, A., A. Kumar, S. A. Munafo, D. Khanduri and M. D. Sevilla (2010) Prototropic
429 equilibria in DNA containing one- electron oxidized GC: intra-duplex vs. duplex to solvent
430 deprotonation. *Phys. Chem. Chem. Phys.* **12,** 5353-5368.
431 34. Kumar, A. and M. D. Sevilla (2011) Density Functional Theory Studies of the Extent of
432 Hole Delocalization in One-Electron Oxidized Adenine and Guanine Base Stacks. *J. Phys.*
433 *Chem. B* **115,** 4990-5000.
434 35. Livshits, G. I., A. Stern, D. Rotem, N. Borovok, G. Eidelshtein, A. Migliore, E. Penzo, S.
435 J. Wind, R. Di Felice, S. S. Skourtis, J. Carlos Cuevas, L. Gurevich, A. B. Kotlyar and D.
436 Porath (2014) Long-range charge transport in single G-quadruplex DNA molecules. *Nat.*
437 *Nanotechnol.* **9,** 1040-1046.
438 36. Capobianco, A., T. Caruso, A. M. D'Ursi, S. Fusco, A. Masi, M. Scrima, C. Chatgilialoglu
439 and A. Peluso (2015) Delocalized Hole Domains in Guanine-Rich DNA Oligonucleotides. *J.*
440 *Phys. Chem. B* **119,** 5462-5466.
441 37. Cadet, J., J. R. Wagner and D. Angelov (2019) Biphotonic Ionization of DNA: From
442 Model Studies to Cell. *Photochem. Photobiol.* **95,** 59-72.
443 38. Candeias, L. P., P. O'Neill, G. D. D. Jones and S. Steenken (1992) Ionization of
444 polynucleotides and DNA in aqueous solution by 193 nm pulsed laser light: identification of
445 base derived radicals. *Int. J. Radiat. Biol.* **61,** 15-20.

446 39. Candeias, L. P. and S. Steenken (1993) Electron transfer in di(deoxy)nucleoside
447 phosphates in aqueous solution: rapid migration of oxidative damage (via adenine) to guanine.
448 *J. Am. Chem. Soc.* **115,** 2437-2440.
449 40. Palecek, E. and M. Bartosik (2012) Electrochemistry of Nucleic Acids. *Chem. Rev.* **112,**
450 3427-3481.
451 41. Kanvah, S., J. Joseph, G. B. Schuster, R. N. Barnett, C. L. Cleveland and U. Landman
452 (2010) Oxidation of DNA: Damage to Nucleobases. *Acc. Chem. Res.* **43,** 280-287.
453 42. Douki, T., D. Angelov and J. Cadet (2001) UV laser photolysis of DNA: effect of duplex
454 stability on charge-transfer efficiency. *J. Am. Chem. Soc.* **123,** 11360-11366.
455 43. Meggers, E., M. E. Michel-Beyerle and B. Giese (1998) Sequence dependent long range
456 hole transport in DNA. *J. Am. Chem. Soc.* **120,** 12950-12955.
457 44. Saito, I., T. Nakamura, K. Nakatani, Y. Yoshioka, K. Yamaguchi and H. Sugiyama (1998)
458 Mapping of the hot spots for DNA damage by one-electron oxidation: Efficacy of GG doublets
459 and GGG triplets as a trap in long-range hole migration. *J. Am. Chem. Soc.* **120,** 12686-12687.
460 45. Genereux, J. C. and J. K. Barton (2010) Mechanisms for DNA Charge Transport. *Chem.*
461 *Rev.* **110,** 1642-1662.
462 46. Kawai, K. and T. Majima (2013) Hole Transfer Kinetics of DNA. *Acc. Chem. Res.* **46,**
463 2616-2625.
464 47. Lewis, F. D., R. L. Letsinger and M. R. Wasielewski (2001) Dynamics of photoinduced
465 charge transfer and hole transport in synthetic DNA hairpins. *Acc. Chem. Res.* **34,** 159-170.
466 48. Chatgilialoglu, C. (2021) The Two Faces of the Guanyl Radical: Molecular Context and
467 Behavior. *Molecules* **26**.

468 49. Merta, T. J., N. E. Geacintov and V. Shafirovich (2019) Generation of 8-oxo-7,8-
469 dihydroguanine in G-Quadruplexes Models of Human Telomere Sequences by One-electron
470 Oxidation. *Photochem. Photobiol.* **95,** 244-251.
471 50. von Sonntag, C. (2006) *Free-Radical-Induced DNA damage and its Repair* Springer-
472 Verlag, Berlin-Heildelberg.
473 51. Peon, J., G. C. Hess, J. M. L. Pecourt, T. Yuzawa and B. Kohler (1999) Ultrafast
474 photoionization dynamics of indole in water. *J. Phys. Chem. A* **103,** 2460-2466.
475 52. Banyasz, A., L. Martinez-Fernandez, R. Improta, T. M. Ketola, C. Balty and D. Markovitsi
476 (2018) Radicals generated in alternating guanine-cytosine duplexes by direct absorption of
477 low-energy UV radiation. *Phys. Chem. Chem. Phys.* **20,** 21381-21389.
478 53. Blumen, A., J. Klafter and G. Zumofen (1986) Models for reaction dynamics in glasses. In
479 *Optical spectroscopy of glasses*. (Edited by I. Zschokke), pp. 199-265. Springer: Dordecht, the
480 Netherlands.
481 54. Li, K., L. Yatsunyk and S. Neidle (2021) Water spines and networks in G-quadruplex
482 structures. *Nucleic Acids Res.* **49,** 519-528.
483 55. Duboue-Dijon, E., A. C. Fogarty, J. T. Hynes and D. Laage (2016) Dynamical Disorder in
484 the DNA Hydration Shell. *J. Am. Chem. Soc.* **138,** 7610-7620.
485 56. Nakano, M., H. Tateishi-Karimata, S. Tanaka, F. Tama, O. Miyashita, S.-i. Nakano and N.
486 Sugimoto (2015) Thermodynamic properties of water molecules in the presence of cosolute
487 depend on DNA structure: a study using grid inhomogeneous solvation theory. *Nucleic Acids*
488 *Res.* **43,** 10114-10125.

57. Phan, A. T., J. L. Leroy and M. Gueron (1999) Determination of the residence time of water molecules hydrating B '-DNA and B-DNA, by one-dimensional zero-enhancement nuclear Overhauser effect spectroscopy. *J. Mol. Biol.* **286,** 505-519.

58. Denisov, V. P., G. Carlstrom, K. Venu and B. Halle (1997) Kinetics of DNA hydration. *J. Mol. Biol.* **268,** 118-136.

59. Snoussi, K. and B. Halle (2008) Internal Sodium Ions and Water Molecules in Guanine Quadruplexes: Magnetic Relaxation Dispersion Studies of d(G(3)T(4)G(3)) (2) and d(G(4)T(4)G(4)) (2). *Biochemistry* **47,** 12219-12229.

60. Benichou, O., C. Chevalier, J. Klafter, B. Meyer and R. Voituriez (2010) Geometry-controlled kinetics. *Nat. Chem.* **2,** 472-477.

61. Bouvier, B., J. P. Dognon, R. Lavery, D. Markovitsi, P. Millié, D. Onidas and K. Zakrzewska (2003) Influence of conformational dynamics on the exciton states of DNA oligomers. *J. Phys. Chem. B* **107,** 13512-13522.

62. Gustavsson, T. and D. Markovitsi (2021) Fundamentals of the Intrinsic DNA Fluorescence. *Acc. Chem. Res.* **54,** 1226-1235.

63. Dai, L., Y. Xu, Z. Du, X.-D. Su and J. Yu (2021) Revealing atomic-scale molecular diffusion of a plant-transcription factor WRKY domain protein along DNA. *Proc. Natl. Acad. Sci. USA* **118**.

64. Armeev, G. A., A. S. Kniazeva, G. A. Komarova, M. P. Kirpichnikov and A. K. Shaytan (2021) Histone dynamics mediate DNA unwrapping and sliding in nucleosomes. *Nature Comm.* **12**.

Table 1. Concentrations of $(G^{+})^{\bullet}$ and $(G\text{-}H2)^{\bullet}$ radicals present in G-Quadruplexes at 3 μs after photoionization, expressed as percentage of $[e_{hyd}^{-}]_0$; error: ≤±5%.

type	Sequence	G-Quadruplex	$(G^{+})^{\bullet}$	$(G\text{-}H2)^{\bullet}$
monomolecular	$TAGGG(TTAGGG)_3TT$	TEL25/Na^{+} † (8)	45	55
	$GGG(TTAGGG)_3$	TEL21/Na^{+} † (7)	50	50
		TEL21/K^{+} † (12)	60	40
bimolecular	GGGGTTTTGGGG	OXY/Na^{+} ††	45	55
		OXY/K^{+} (13) ††	30	70
tetramolecular	TGGGGT	$(TG_4T)_4$/Na^{+} (9)	25	75
		$(TG_4T)_4$/K^{+} (11)	40	60

†TEL: containing the human telomeric repeat TTAGGG; ††OXY: containing the oxytricha nova telomeric repeat TTTTGGGG.

FIGURE CAPTIONS

Figure 1. Schematic illustration of the G-Quadruplexes discussed in this review: (a) monomolecular, formed by folding of a single strand, (b) bimolecular, formed by folding and association of two single strands and (c) tetramolecular, formed by association of four single strands; red spheres represent metal cations (Na^+, K^+) located in the central cavity. Guanines are shown in violet and the backbone in grey.

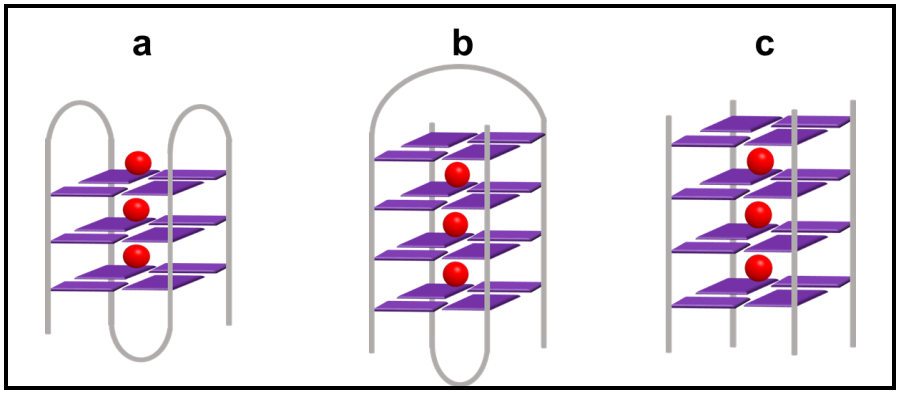

Figure 2. Spectral differences corresponding to $(G^+)^\bullet \rightarrow (G\text{-}H1)^\bullet$ (a) and $(G^+)^\bullet \rightarrow (G\text{-}H2)^\bullet$ (b) deprotonation, obtained by subtracting the spectrum of the radical cation from those of deprotonated radicals determined for monomeric guanosine derivatives (2, 48). The position of H1 and H2 hydrogen atoms is indicated in the insets.

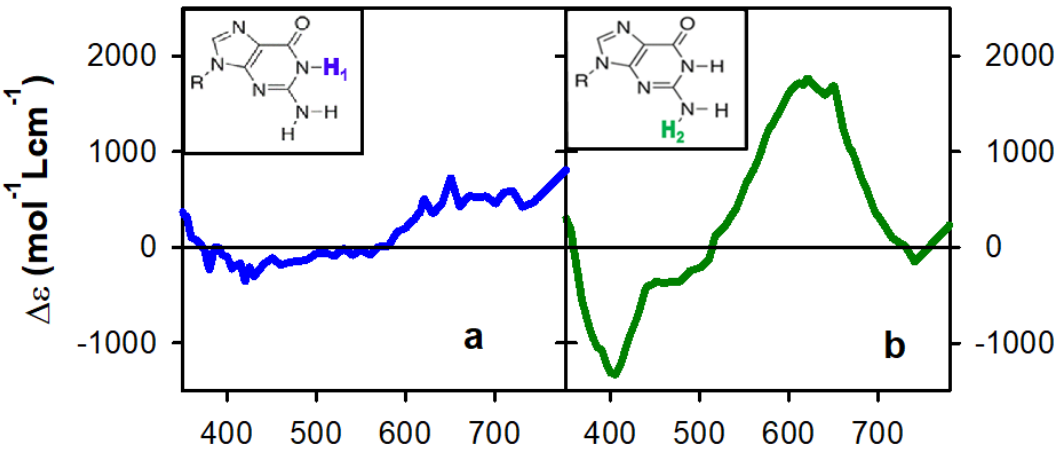

530 **Figure 3**. Location of the hydrogen atoms H1 and H2 in (a) a Watson-Crick guanine-cytosine
531 pair; (b) a tetrad composed of four guanines interconnected via Hoogsteen hydrogen bonds.

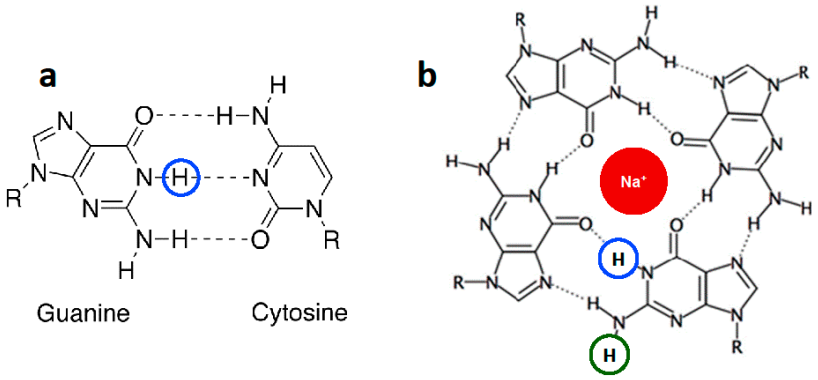

532

533 **Figure 4**. Transient absorption signals (black) recorded for N_2O-saturated solutions of CT-
534 DNA at 700 nm. The red line in (a) is derived from a fit with the model function A_1 (1-exp(-
535 t/τ_1))+A_0 with τ_1 = 320 ± 30 ns. Adapted from reference 9 with ACS permission.

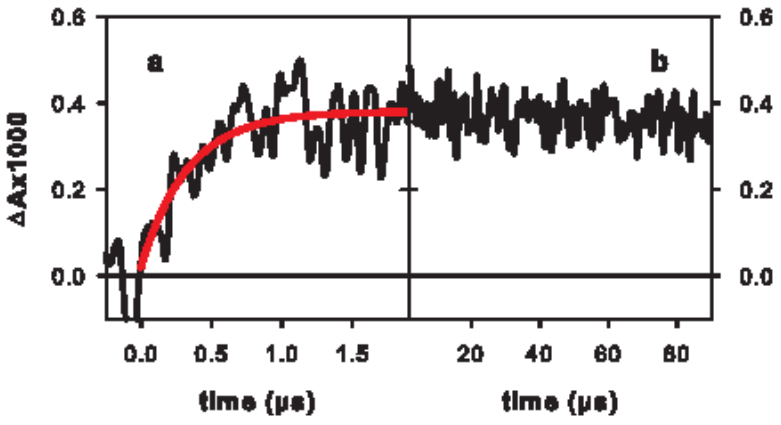

536

537

Figure 5. Reconstruction of the transient absorption spectra determined for G-Quadruplexes (circles) with linear combinations of the $(G^{+})^{\bullet}$ and $(G\text{-}H2)^{\bullet}$ spectra reported for monomeric guanosine derivatives (solid lines), represented with their molar absorption coefficient (26, 48). (a) OXY/Na^{+} at 3 µs; $[(G^{+})^{\bullet}]/[(G\text{-}H2)^{\bullet}] = 45/55$, $[(G^{+})^{\bullet}] + [(G\text{-}H2)^{\bullet}] = [e_{hyd}^{-}]_0$. (b) TEL21/$Na^{+}$ at 25 µs; $[(G^{+})^{\bullet}]/[(G\text{-}H2)^{\bullet}] = 20/80$, $[(G^{+})^{\bullet}] + [(G\text{-}H2)^{\bullet}] = 0.85[e_{hyd}^{-}]_0$.

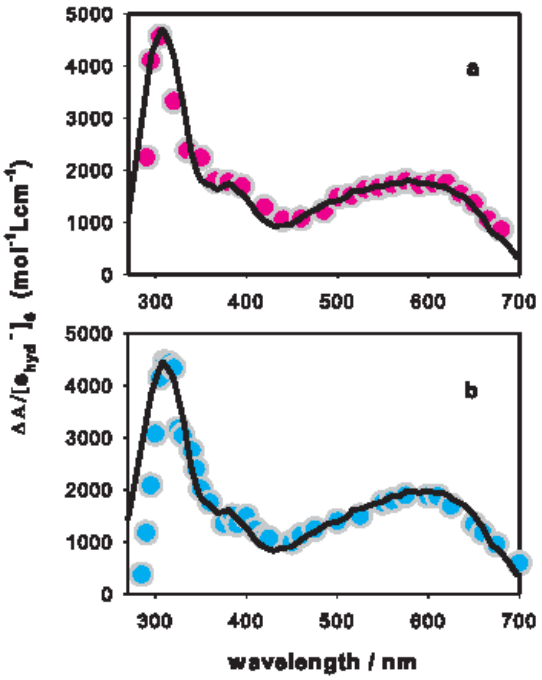

Figure 6. Deprotonation of in G-Quadruplexes on the sub-microsecond time scale. Transient absorption signals recorded for N_2O-saturated solutions of TEL21/K^{+} (red) (12), OXY/Na^{+} (green) and OXY/K^{+} (pink) (13). Yellow lines correspond to fits with mono-exponential functions, A_1 (1-exp(-t/τ))+A_0; τ = 150 ± 15 ns (a) and 200 ± 30 ns (b; adapted from reference (13) with ACS permission).

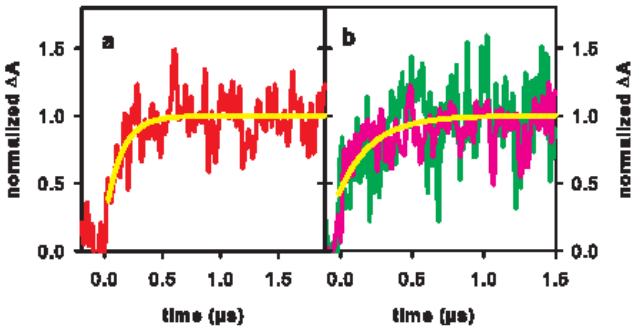
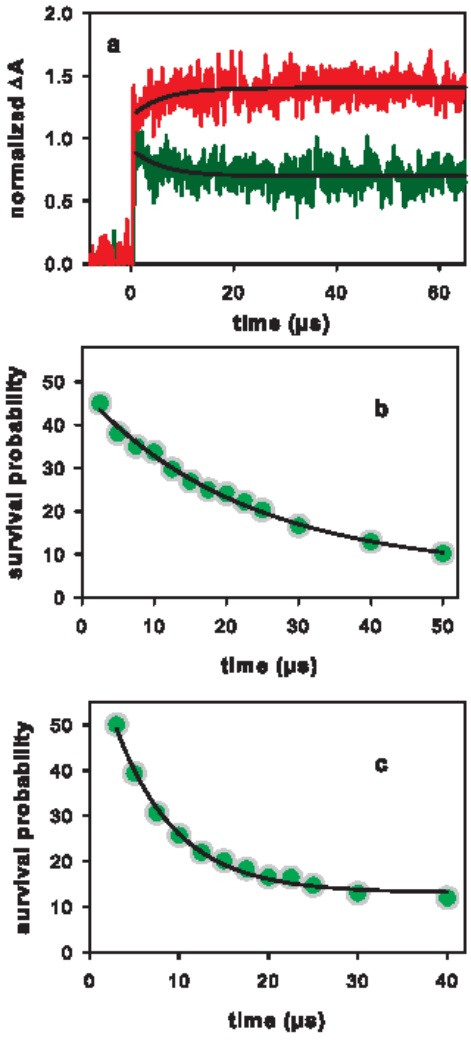
Figure 7. Reaction dynamics of $(G^+)^\bullet$ in G-Quadruplexes on the microsecond time-scale. (a) transient absorption signals recorded at 500 nm (green) and 600 nm (red) for $(TG_4T)_4/Na^+$; their intensity has been arbitrarily scaled; reproduced from reference 24 with ACS permission. Survival probability of the $(G^+)^\bullet$ population (circles) in OXY/Na^+ (b) and TEL21/Na^+ (c), determined from reconstruction of the time-resolved spectra, as shown in Figure 5. Black lines correspond to fits with exponential functions $A_1(1-\exp(t/\tau_1))+A_0$ (rise) and $A_1\exp(-t/\tau_2)+A_0$ (decays) with time constants: 6 ± 1 μs (a); 22 ± 2 μs (b) and 7 ± 0.5 μs (c).